THE JOURNAL OF
PHYSICAL CHEMISTRY A
Article
Cite This: J. Phys. Chem. A 2019, 123, 4755−4763
pubs.acs.org/JPCA

Variationally Computed IR Line List for the Methyl Radical CH_3

Ahmad Y. Adam,[†] Andrey Yachmenev,[‡,§] Sergei N. Yurchenko,[∥] and Per Jensen*[,†]

[†]Fakultät für Mathematik und Naturwissenschaften, Physikalische und Theoretische Chemie, Bergische Universität Wuppertal, D-42097 Wuppertal, Germany

[‡]Center for Free-Electron Laser Science, Deutsches Elektronen-Synchrotron DESY, Notkestraβe 85, D-22607 Hamburg, Germany

[§]The Hamburg Center for Ultrafast Imaging, Universität Hamburg, Luruper Chaussee 149, D-22761 Hamburg, Germany

[∥]Department of Physics and Astronomy, University College London, Gower Street, WC1E 6BT London, U.K.

Supporting Information

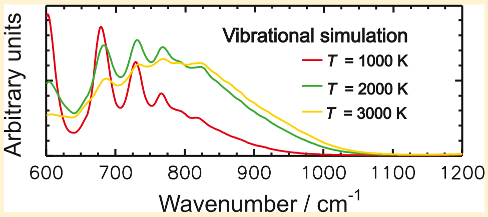

ABSTRACT: We present the first variational calculation of a hot-temperature ab initio line list for the CH_3 radical. It is based on a high-level ab initio potential energy surface and dipole moment surface of CH_3 in the ground electronic state. The ro-vibrational energy levels and Einstein A coefficients were calculated using the general-molecule variational approach implemented in the computer program TROVE. Vibrational energies and vibrational intensities are found to be in very good agreement with the available experimental data. The line list comprises 9 127 123 ro-vibrational states ($J \leq 40$) and 2 058 655 166 transitions, covering the wavenumber range up to 10 000 cm^{-1} and should be suitable for temperatures up to T = 1500 K.

INTRODUCTION

The methyl radical CH_3 is a free radical of major importance in many areas of science, such as hydrocarbon combustion processes,[1] atmospheric chemistry,[2] the chemistry of semiconductor production,[3] the chemical vapor deposition of diamond,[4] and many chemical processes of current industrial and environmental interest. It is also expected to be present in exo-planetary atmospheres,[5] in the atmospheres of Saturn[6] and Neptune,[7] and in the interstellar medium,[8] where it is thought to be one of the most abundant free radicals.[5] Because of its central role in this variety of situations, its structural and spectroscopic parameters have been extensively studied. Diverse spectroscopic techniques have been employed to determine absolute concentrations of CH_3 in the gas phase, including UV/visible,[9] infrared,[10] and Raman spectroscopies.[11−17] In addition, CH_3 is an example of a molecule with large vibrational contribution to the hyperfine coupling constant, accounting for up to about 41% of the total value (see ref 18 and references therein).

Owing to the importance of CH_3 in various contexts, in particular in astrophysics and astrochemistry, its concentrations or column densities in remote environments, such as interstellar space, terrestrial atmosphere, exo-planetary atmospheres, and the outer layers of cool stars, are of interest, and it is desirable to determine these by remote-sensing spectroscopic methods. A prerequisite for such determinations is the knowledge of the transition moments for the observed transitions, and these must often be obtained in theoretical calculations as done, for example, in the ExoMol project[19,20] by Yurchenko, Tennyson, and co-workers.[21−33] This project aims at providing theoretically computed transition moments and simulated spectra for (small to medium-sized) general polyatomic molecules of astrophysical and/or astrochemical interest. In general, molecular transition moments known to be within 10−20% (the typical accuracy of the transition moment data of the HITRAN database[34]) are sufficiently accurate to be useful for most applications involving the determination of concentrations and column densities, at least for fundamental and overtone bands. The level of ab initio theory used in the present study [RCCSD(T)-F12b/cc-pVQZ-F12; see below] is expected to be sufficient to satisfy this requirement for the transition moments computed in the present work. Also, we expect the inaccuracy of our calculations to be predominantly caused by the inaccuracy of the ab initio potential energy surface (PES), and not by the truncation of the kinetic energy operator expansion.

At equilibrium, the three protons of electronic ground state $\tilde{X}\,^2A_2''$ CH_3 form an equilateral triangle with the C nucleus at the center of mass of the planar structure with D_{3h} point group symmetry (see Table A-10 of ref 35). There is no permanent dipole moment, and so the pure rotational transitions are dipole forbidden and very weak. Also, the planar ground-state equilibrium structure precludes most one-photon transitions to excited electronic states.[36] Owing to the extremely weak rotational spectrum, determinations of concentrations and column densities for CH_3 must be made with ro-vibrational transitions in the infrared region. The most suitable transitions are those in the intense ν_2 fundamental band at 606 cm^{-1} (where ν_2 is the out-of-plane bending mode). This band provides convenient transitions for concentration measure-

Received: March 28, 2019
Revised: May 2, 2019
Published: May 3, 2019

DOI: 10.1021/acs.jpca.9b02919
J. Phys. Chem. A 2019, 123, 4755−4763

ments and has been used extensively for this purpose.[37−40] As mentioned above, the corresponding transition moments must be known in order that concentrations can be determined, and the present work can be viewed as a first step toward providing extensive catalogs of theoretical transition moments for CH_3, so-called line lists, of use in astrophysical studies. In the present work, we apply a high-level ab initio PES, refined by means of experimental spectroscopic data, and ab initio dipole moment surfaces (DMSs) to compute, with the TROVE program,[41−44] sufficient energies and transition moments for generating a hot (T = 1500 K) IR line list for CH_3.

■ THEORY

Potential Energy Surface. The PES employed for the electronic ground state of CH_3 in the present work is based on the ab initio surface reported in ref 18, which we denote as PES-1. The PES-1 electronic energies were computed for 24 000 symmetry-unique molecular geometries at the open-shell RCCSD(T)-F12b[45,46] level of theory (explicitly correlated F12-restricted coupled cluster included single and double excitations with a noniterative correction for triples) and the F12-optimized correlation consistent polarized valence basis set cc-pVQZ-F12.[47] The carbon inner-shell electron pair was treated as a frozen core in the correlated calculations. By using the frozen-core approximation, we benefit from error cancelation. It is well known that, for example, for second-row atoms, the core-valence correlation is almost exactly canceled by the more costly high-order correlation effects.[48] Keeping only one of them would make the accuracy deteriorate.

The analytical representation for the PES was obtained in a least-squares fitting procedure using the parameterized function from Lin et al.[49]

$$\begin{aligned} V(\xi_1, \xi_2, \xi_3, \xi_{4a}, \xi_{4b}; \sin\bar{\rho}) &= V_e + V_0(\sin\bar{\rho}) + \sum_j F_j(\sin\bar{\rho})\xi_j \\ &+ \sum_{j\le k} F_{jk}(\sin\bar{\rho})\xi_j\xi_k + \sum_{j\le k\le l} F_{jkl}(\sin\bar{\rho})\xi_j\xi_k\xi_l \\ &+ \sum_{j\le k\le l\le m} F_{jklm}(\sin\bar{\rho})\xi_j\xi_k\xi_l\xi_m + \ldots \end{aligned} \tag{1}$$

This function depends on the stretching variables

$$\xi_k = 1 - \exp[-a(r_k - r_e)],\ \ k = 1, 2, 3 \tag{2}$$

where r_k is the instantaneous value of the distance between the C nucleus and the proton H_k labeled k = 1, 2, or 3; r_e is the common equilibrium value of the three r_k bond lengths; and a is a Morse parameter. Furthermore, the symmetrized bending variables (ξ_{4a}, ξ_{4b}) are defined as

$$(\xi_{4a}, \xi_{4b}) = \left(\frac{1}{\sqrt{6}}[2\alpha_1 - \alpha_2 - \alpha_3], \frac{1}{\sqrt{2}}[\alpha_2 - \alpha_3]\right) \tag{3}$$

with α_i as the bond angle $\angle(H_jXH_k)$, where (i, j, k) is a permutation of the numbers (1, 2, 3). Finally, the variable

$$\sin\bar{\rho} = \frac{2}{\sqrt{3}}\sin[(\alpha_1 + \alpha_2 + \alpha_3)/6] \tag{4}$$

describes the out-of-plane bending. At the planar equilibrium configuration, we have $\alpha_1 + \alpha_2 + \alpha_3 = 360°$ and so $\sin\bar{\rho} = \sin\bar{\rho}_e = 1$. The functions $V_0(\sin\bar{\rho})$ and $F_{jk\ldots}(\sin\bar{\rho})$ in eq 1 are defined as

$$V_0(\sin\bar{\rho}) = \sum_{s=1}^{4} f_0^{(s)}(1 - \sin\bar{\rho})^s \tag{5}$$

$$F_{jk\ldots}(\sin\bar{\rho}) = \sum_{s=0}^{N} f_{jk\ldots}^{(s)}(1 - \sin\bar{\rho})^s \tag{6}$$

where the quantities $f_0^{(s)}$ and $f_{jk\ldots}^{(s)}$ in eqs 5 and 6 are expansion coefficients. The optimized values of the parameters a, r_e, $f_0^{(s)}$, and $f_{jk\ldots}^{(s)}$ are given in the Supporting Information to ref 18 together with Fortran 90 routine for calculating PES values.

The analytical form of PES-1[18] is given in terms of the ab initio cc-pVQZ-F12 values of the equilibrium structural parameters, r_e = 1.0774 Å and α_e = 120°,[18] for the electronic ground state of CH_3. In the present work, we optimized the value of r_e in a least-squares fitting to experimentally derived rotational energy spacings within the vibrational states of CH_3. The fitting produced r_e = 1.0763 Å; α_e = 120° by symmetry. We use these optimized values of the equilibrium structural parameters. All results presented below are based on the analytical potential energy function called PES-2, obtained from PES-1[18] by replacing the ab initio cc-pVQZ-F12 value of r_e by the adjusted value given here. The remaining PES-2 parameter values are identical to those of PES-1 and can be obtained from the Supporting Information to ref 18.

Dipole Moment Surface. The DMS for the electronic ground state of CH_3 was computed using the MOLPRO[50] program package. Frozen-core calculations were carried out for 19 361 symmetry-unique geometries (15 600 below 30 000 cm^{-1}) using the spin-restricted open-shell coupled cluster theory RCCSD(T)[51] and the augmented correlation consistent valence basis set aug-cc-pVTZ,[52,53] employing the two-point stencil central finite differences with the electric field strength of 0.002 a.u.

We employ the so-called symmetrized molecular-bond (SMB) representation[22] [which is an extension of the molecular-bond (MB) representation[54] to formulate analytical functions describing the molecular dipole moment components. The SMB representation makes use of the projections $\bar{\boldsymbol{\mu}}\cdot\mathbf{e}_k$ of the dipole moment on the molecular bonds, where $\mathbf{e}_k$ is the unit vector along the C−H_k bond

$$\mathbf{e}_k = \frac{\mathbf{r}_k - \mathbf{r}_4}{|\mathbf{r}_k - \mathbf{r}_4|} \tag{7}$$

where $\mathbf{r}_k$ (k = 1, 2, 3) is the position vector of proton k and $\mathbf{r}_4$ is the position vector of the C nucleus.

We form symmetry-adapted linear combinations of the MB projections $\bar{\boldsymbol{\mu}}\cdot\mathbf{e}_j$

$$\bar{\mu}_{A_2''}^{\mathrm{SMB}} = (\bar{\boldsymbol{\mu}}\cdot\mathbf{e}_N) \tag{8}$$

$$\bar{\mu}_{E_a'}^{\mathrm{SMB}} = \frac{1}{\sqrt{6}}[2(\bar{\boldsymbol{\mu}}\cdot\mathbf{e}_1) - (\bar{\boldsymbol{\mu}}\cdot\mathbf{e}_2) - (\bar{\boldsymbol{\mu}}\cdot\mathbf{e}_3)] \tag{9}$$

$$\bar{\mu}_{E_b'}^{\mathrm{SMB}} = \frac{1}{\sqrt{2}}[(\bar{\boldsymbol{\mu}}\cdot\mathbf{e}_2) - (\bar{\boldsymbol{\mu}}\cdot\mathbf{e}_3)] \tag{10}$$

where, in addition to the vectors $\mathbf{e}_k$, we have introduced $\mathbf{e}_N = \mathbf{q}_N/|\mathbf{q}_N|$ with $\mathbf{q}_N$ as the "trisector"

$$\mathbf{q}_N = (\mathbf{e}_1 \times \mathbf{e}_2) + (\mathbf{e}_2 \times \mathbf{e}_3) + (\mathbf{e}_3 \times \mathbf{e}_1) \tag{11}$$

The subscripts $\Gamma = A_2''$, E_a', and E_b' of the quantities $\bar{\mu}_\Gamma^{\mathrm{SMB}}$ in eqs 8−10 refer to the irreducible representations (Table A-10 of ref 35) of the CH_3 molecular symmetry group D_{3h}(M); the electronically averaged dipole moment $\bar{\boldsymbol{\mu}}$ generates the representation $A_2'' \oplus E'$. The quantity $\bar{\mu}_{A_2''}^{\rm SMB}$ is antisymmetric under the inversion operation[35] E^* and vanishes at planarity, so that $\bar{\boldsymbol{\mu}}$ has only two non-vanishing, linearly independent components at planarity. These two components vanish at planar configurations with D_{3h} point group symmetry.

The three components of the SMB dipole moment in eqs 8−10 are represented by 4th-order polynomial expansions

$$\begin{aligned}\bar{\mu}_\Gamma^{\rm SMB}&(\chi_1, \chi_2, \chi_3, \chi_{4a}, \chi_{4b}; \rho)\\ &= \mu_0^\Gamma(\sin\bar{\rho}) + \sum_i \mu_i^\Gamma(\sin\bar{\rho})\chi_i + \sum_{i\le j}\mu_{ij}^\Gamma(\sin\bar{\rho})\chi_i\chi_j\\ &\quad + \sum_{i\le j\le k}\mu_{ijk}^\Gamma(\sin\bar{\rho})\chi_i\chi_j\chi_k + \sum_{i\le j\le k\le l}\mu_{ijkl}^\Gamma(\sin\bar{\rho})\chi_i\chi_j\chi_k\chi_l\end{aligned} \tag{12}$$

in terms of the variables

$$\chi_k = \Delta r_k \exp(-(\Delta r_k)^2), \qquad (k = 1, 2, 3) \tag{13}$$

with $\Delta r_k = r_k - r_{\rm e}$ and

$$(\chi_4, \chi_5) = (\xi_{4a}, \xi_{4b}) \tag{14}$$

where (ξ_{4a}, ξ_{4b}) are defined in eq 3. The expansion coefficients $\mu_{ij...}^\Gamma(\sin\bar{\rho})$ are defined as

$$\mu_{ij...}^\Gamma(\sin\bar{\rho}) = \sum_{s=0}^{N} \mu_{ij...}^{\Gamma(s)}(1 - \sin\bar{\rho})^s \tag{15}$$

where $\sin\bar{\rho}$ is given by eq 4 and the maximal order of the polynomial is $N = 8$. For more details the reader is referred to ref 22. The final fit of the 15 600 geometries required a total number of 218 parameters (131 for $\bar{\mu}_{A_2''}^{\rm SMB}$ and 87 for $\bar{\mu}_{E_a'}^{\rm SMB}$ and $\bar{\mu}_{E_b'}^{\rm SMB}$) and reproduced the ab initio data with root-mean-square (rms) differences of 0.003, 0.001, and 0.004 D for the x, y, and z components, respectively, and energies up to 30 000 cm^{-1}; see Figure 1. A series of fittings to the x, y, and z ab initio dipole-moment components have been carried out, including in the data set for each fitting the ab initio points with electronic energy (relative to the potential energy minimum) $V \le E$ and increasing E. Figure 1 shows the rms deviation for each dipole-moment component as a function of E. The DMS expansion parameter set and the Fortran 90 functions are included in the Supporting Information.

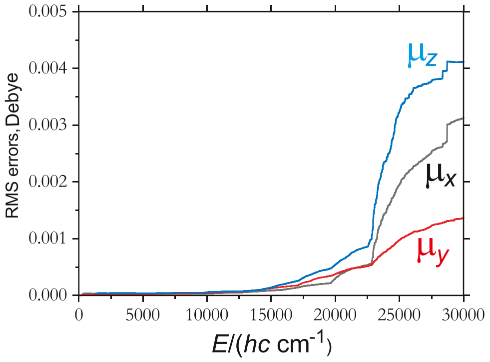

Figure 1. rms errors of the fittings to the ab initio dipole moment values. The results of a series of fittings are shown. In each fitting, the data set includes the ab initio points with electronic energy (relative to the potential energy minimum) $V \le E$ (see text).

Intensity Simulations with TROVE. The "readiness" of the molecule to make an absorption or emission transition from an initial ro-vibrational state i to a final ro-vibrational state f is expressed by the line strength[35,55,56] $S({\rm f} \leftarrow {\rm i})$, a quantity with units of [dipole moment]^2 (typically Debye^2). For $S({\rm f} \leftarrow {\rm i}) = 0$, the transition does not take place and need not be considered. As discussed in ref 35, transitions with $S({\rm f} \leftarrow {\rm i}) \neq 0$ are said to satisfy selection rules, which we can derive from symmetry considerations before we do quantitative, numerical calculations of $S({\rm f} \leftarrow {\rm i})$. Thus, these calculations need only be done for transitions satisfying the selection rules, and after obtaining values of $S({\rm f} \leftarrow {\rm i})$ for these transitions, we can compute the corresponding Einstein coefficients and absorption intensities.

The initial(final) state i(f) has the rotation−vibration wavefunction $|\Phi_{\rm rv}^{(\rm i)}\rangle (|\Phi_{\rm rv}^{(\rm f)}\rangle)$. The line strength[35,55,56] $S({\rm f} \leftarrow {\rm i})$ of the ro-vibrational transition f ← i is

$$S({\rm f} \leftarrow {\rm i}) = g_{\rm ns} \sum_{M_{\rm f}, M_{\rm i}} \sum_{A=X,Y,Z} |\langle \Phi_{\rm rv}^{(\rm f)} | \bar{\mu}_A | \Phi_{\rm rv}^{(\rm i)} \rangle|^2 \tag{16}$$

where the nuclear spin statistical weight factor[35] is denoted as $g_{\rm ns}$ and the electronically averaged component of the molecular dipole moment along the space-fixed axis[35] is denoted as $\bar{\mu}_A$, $A = X$, Y, or Z. The quantity $M_{\rm i}(M_{\rm f})$ is the quantum number defining the projection of the total angular momentum $\hat{\mathbf{J}}$ on the Z axis for the initial(final) state.

Assuming that the molecules considered are in thermal equilibrium at the absolute temperature T, the intensity of a spectral line is determined as

$$I({\rm f} \leftarrow {\rm i}) = \frac{8\pi^3 N_{\rm A} \tilde{\nu}_{\rm if}}{(4\pi\varepsilon_0)3hc} \frac{{\rm e}^{-E_{\rm i}/kT}}{Q}[1 - \exp(-hc\tilde{\nu}_{\rm if}/kT)] S({\rm f} \leftarrow {\rm i}) \tag{17}$$

Here, the absorption wavenumber is denoted as $\tilde{\nu}$, and eq 17 yields the intensity of a transition from the initial state i with energy $E_{\rm i}$ to the final state f with energy $E_{\rm f}$, where $hc\tilde{\nu}_{if} = E_{\rm f} - E_{\rm i}$. The partition function Q is defined as $Q = \sum_j g_j \exp(-E_j/kT)$, where g_j is the total degeneracy of the state with energy E_j and the sum runs over all energy levels of the molecule, and other symbols have their usual meanings. The total degeneracy g_j is given by $(2J + 1)$ times the spin degeneracy and $(2S + 1 = 2)$ times the nuclear spin degeneracy, which is 4, 0, 2, 4, 0, 2 for A_1', A_2', E', A_1'', A_2'', and E'' symmetries, respectively. The ground electronic state of CH$_3$ is a doublet ($\tilde{X}\ ^2A_2''$) with a small splitting[57,58] in the ro-vibrational energy levels because of spin-rotation interactions, around 0.01 cm^{-1}, which we therefore chose to ignore in the present work.

Yurchenko et al.[55] have given, in their eq 21, a detailed expression for the line strength of an individual ro-vibrational transition within an isolated electronic state of an XY_3 pyramidal molecule. Assuming that the populations of the lower (initial) states are Boltzmann distributed, we limit the intensity calculations to transitions starting from levels below $E_i^{\rm max}/hc = 9000$ cm^{-1}. With this limitation, Boltzmann factors of $\exp(-E_i/kT) > 2 \times 10^{-4}$ enter into eq 17 for $T = 1500$ K. It is common to use the partition function for estimating the completeness of the line list for a given temperature.[24] Toward this end, we consider the ratio $Q_{9000{\rm cm}^{-1}}/Q_{\rm total}$, where $Q_{\rm total}$ is the converged partition function value calculated by explicit summation over all computed energy levels and $Q_{9000{\rm cm}^{-1}}$ is the partition function value calculated by summation over levels with energies lower than 9000 cm^{-1}. This ratio gives 95% completeness at temperatures below 1500 K. Consequently, we estimate T = 1500 K to be the maximal temperature for which our line list is realistic. Because it is safe to limit the lower-state energies to be below 9000 cm^{-1}, it is sufficient to consider rotational states with $J \leq 40$. We compute a line list in the wavenumber range 0−10 000 cm^{-1}; the upper energy limit (i.e., the maximum value of the final-state energy) corresponds to a term value of E^{max}/hc = 19 000 cm^{-1}.

■ COMPUTATIONAL DETAILS

The variational nuclear-motion calculations are done with a symmetry-adapted basis set. With such a basis set, the Hamiltonian matrix becomes block diagonal according to the irreducible representations of the D_{3h}(M) molecular symmetry group:[35] A_1', A_2', A_1'', A_2'', E', and E''. The A_2' and A_2'' matrices are of no interest for CH$_3$ as the corresponding states have zero nuclear spin statistical weights and do not exist in nature.[35] The E' and E'' matrices each split into two sub-blocks, of which only one must be diagonalized.[35]

The calculation of the matrix elements $\langle\Phi^{(\mathrm{f})}_{\mathrm{rv}}|\bar{\mu}_A|\Phi^{(\mathrm{i})}_{\mathrm{rv}}\rangle$ in eq 16 is the bottleneck in the spectrum simulations. Here, the wavefunctions $\Phi^{(\mathrm{w})}_{\mathrm{rv}}$ are given as superpositions of symmetry-adapted basis functions (see eq 65 of Yurchenko et al.[44])

$$|\Phi^{(\mathrm{w})}_{\mathrm{rv}}\rangle = \sum_{VK\tau_{\mathrm{rot}}} C^{(\mathrm{w})}_{VK\tau_{\mathrm{rot}}} |J_{\mathrm{w}} K m_{\mathrm{w}} \tau_{\mathrm{rot}}\rangle |V\rangle, \qquad \mathrm{w} = \mathrm{i\ or\ f} \tag{18}$$

with $C^{(\mathrm{w})}_{VK\tau_{\mathrm{rot}}}$ as expansion coefficients. In eq 18, the symmetrized rotational basis functions are denoted $|J_{\mathrm{w}}\ K\ m_{\mathrm{w}}\ \tau_{\mathrm{rot}}\rangle$ with τ_{rot} (=0 or 1) defining the rotational parity, and $|V\rangle$ is a vibrational basis function. In order to accelerate this part of the calculation, we pre-screened the expansion coefficients $C^{(\mathrm{f})}_{VK\tau_{\mathrm{rot}}}$. All terms with coefficients less than the threshold value of 10^{-13} were discarded in the intensity calculation.

The evaluation of the dipole moment matrix elements $\langle\Phi^{(\mathrm{f})}_{\mathrm{rv}}|\bar{\mu}_A|\Phi^{(\mathrm{i})}_{\mathrm{rv}}\rangle$ has been made more efficient in a two-step procedure. In the first step, an effective line strength is evaluated for a given lower state i

$$S^{A}_{\mathrm{i},VK} = \langle\Phi^{(\mathrm{i})}_{\mathrm{rv}}|\bar{\mu}_A|\phi_{VK}\rangle \tag{19}$$

Here, ϕ_{VK} is a short-hand notation for the primitive basis function $|J_{\mathrm{w}}\ K\ m_{\mathrm{w}}\ \tau_{\mathrm{rot}}\rangle \times |V\rangle$. From the $S_{i,VK}$ values obtained, we compute, in the second step, the line strength $S(\mathrm{f} \leftarrow \mathrm{i})$ as

$$S(\mathrm{f} \leftarrow \mathrm{i}) = g_{\mathrm{ns}} \sum_{m_{\mathrm{i}},m_{\mathrm{f}}} \sum_{A=X,Y,Z} \left| \sum_{V,K} C^{(\mathrm{f})}_{VK\tau_{\mathrm{rot}}} S^{A}_{\mathrm{i},VK} \right|^2 \tag{20}$$

We had to compute a very large number of transitions satisfying the selection rule $|J_{\mathrm{f}} - J_{\mathrm{i}}| \leq 1$, where J_{i} and J_{f} are the values of the angular momentum quantum number J for the initial and final state, respectively. Consequently, we saved memory by organizing the calculation of the ro-vibrational eigenstates and the $S(\mathrm{f} \leftarrow \mathrm{i})$-values, such that at a given time, only eigenvectors for states with two consecutive J values, J and $J + 1$, are available for the computation of $S(\mathrm{f} \leftarrow \mathrm{i})$ values. This algorithm is implemented in the GPU GAIN-MPI program.[59]

The vibrational basis set $|V\rangle$ is obtained in TROVE using a multistep contraction and symmetrization procedure, starting from local primitive basis set functions, each depending on one variable only (see refs[42−44] and references therein). Thus, a compact representation of the vibrational basis set is obtained in a form optimized for the molecule of interest. The final vibrational basis set is represented by the eigenfunctions of the purely vibrational part of the Hamiltonian; we call these eigenfunctions the "J = 0 basis".

■ RESULTS

Basis Set Convergence and Empirical Adjustment of the Vibrational Band Centers. The dimensions of the Hamiltonian matrix blocks to be diagonalized are important in determining the accuracy of the computed energies and wavefunctions for highly excited ro-vibrational states. Consequently, it is imperative to determine empirically the smallest basis set with which the required eigenvalue accuracy (i.e., the optimum basis-set size for "convergence") can be attained.

In TROVE, the size of the vibrational basis set is controlled by polyad number truncation.[41−43] For CH$_3$, the polyad number P is defined as

$$P = 2(n_1 + n_2 + n_3) + n_4 + n_5 + n_6 \tag{21}$$

where n_i are the principal quantum numbers associated with the primitive functions $\phi_{n_i}(\xi_i)$. The primitive vibrational basis functions are products of one-dimensional basis functions $\phi_{n_i}(\xi_i)$, and only products with $P \leq P_{\mathrm{max}}$ are included in the primitive vibrational basis.

An even tighter level of convergence could be achieved for the vibrational term values if these were calculated with different P_{max} values and the resulting progression of term values were extrapolated to the complete vibrational basis set limit.[60] However, for the purpose of generating line lists, this is not considered necessary. The corrections from the extrapolation will be small compared with the term-value errors caused by the imperfection of the underlying PES. Instead, we pragmatically aim for a higher accuracy by resorting to an empirical approach: the theoretical vibrational term values are replaced by the available accurate, experimentally derived vibrational band-center values. In this manner, we are adjusting the vibrational band centers "manually"; this empirical adjustment also shifts the rotational energy-level structure toward better agreement with experiment. We call this procedure the EBSC scheme as it can be regarded as an empirical basis-set correction.

We adopt the EBSC scheme for the vibrational bands ν_2, $2\nu_2$, ν_1, ν_4^1, and ν_3^1, for which accurate experimental data are available, in combination with PES-2, where we have adjusted the equilibrium structure of the molecule to fit the experimentally derived pure rotational term values. The vibrational basis set was truncated at the polyad number P_{max} = 32. We incorporate experimental information in the EBSC scheme, and so we obviously depart from a purely ab initio approach. This is considered justified by the accuracy improvement that can be achieved in the computation of an extensive ro-vibrational line list.

To improve the accuracy of the predicted vibrational band centers, a more thorough refinement of the PES would be required. However, the available accurate experimental data for the vibrationally excited states of CH$_3$ are severely limited, and so we opted for the EBSC approach in conjunction with the r_{e} refinement. For all bands that are not EBSC corrected, the predicted vibrational term values are determined to a significant extent by the ab initio data, and so their accuracy is limited. However, we have improved the prediction of the rotational structures, and that will facilitate the assignments of future experimental spectra for CH_3.

In Table 1, the vibrational term values below 5000 cm^{-1} of the methyl radical, calculated variationally in the present work from PES-2, are compared with the available experimental data. The EBSC substitution was made in the $J > 0$ TROVE calculations of the present work, in that the theoretical vibrational term values (obtained for $P_{max} = 32$) were replaced by the experimental values in Table 1. This table also shows the effect of the polyad number P_{max} on the vibrational energy.

Table 1. Vibrational Band Centers (cm^{-1}) of $^{12}CH_3$ from Variational Calculations

Γ	state	ref	obs.[a]	$P_{max} = 24$[b]	$P_{max} = 32$[c]
A_1'	$2\nu_2$	61	1288.1	1279.77	1281.24
	$2\nu_4$			2737.63	2739.64
	$4\nu_2$			2773.65	2776.86
	ν_1	13	3004.42	3002.71	3002.76
	$3\nu_4^3$			4118.59	4120.58
	$\nu_1 + 2\nu_2$			4258.97	4260.53
	$6\nu_2$			4391.99	4397.00
	$\nu_3^1 + \nu_4^1$			4537.94	4538.93
	$4\nu_4$			5371.39	5364.56
	$2\nu_2 + 3\nu_4^3$			5475.84	5480.07
	$4\nu_2 + 2\nu_4$			5601.91	5607.20
E'	ν_4^1	62	1397.0	1385.99	1387.26
	$2\nu_2 + \nu_4^1$			2688.80	2691.61
	$2\nu_4^2$			2759.77	2762.05
	ν_3^1	58	3160.8	3158.88	3158.83
	$3\nu_4^1$			4074.69	4075.46
	$2\nu_2 + 2\nu_4^2$			4087.92	4091.72
A_2''	ν_2	13	606.453	602.43	602.43
	$3\nu_2$			2010.09	2010.09
	$\nu_2 + 2\nu_4^0$			3372.27	3371.59
	$5\nu_2$			3569.96	3569.95
	$\nu_1 + \nu_2$			3596.35	3596.30
	$3\nu_4^3$			4768.70	4767.06
	$\nu_2 + 2\nu_4^0$			4823.32	4822.79
	$\nu_1 + 3\nu_2$			4981.58	4981.52
E''	$\nu_2 + \nu_4^1$			2000.24	2002.22
	$\nu_2 + 2\nu_4^2$			3388.24	3391.11
	$3\nu_2 + \nu_4^1$			3426.45	3430.06
	$\nu_2 + \nu_3^1$			3736.40	3736.97
	$\nu_2 + 3\nu_4^1$			4726.62	4728.62
	$3\nu_2 + 2\nu_4^2$			4835.22	4839.85
	$\nu_1 + \nu_2 + \nu_4^1$			4980.92	4983.16

[a] Experimental values of band centers used to replace the theoretical values $P_{max} = 32$; see text. [b] Computed using the $P_{max} = 24$ basis set in conjunction with PES-2.[18] [c] Computed using the $P_{max} = 32$ basis set in conjunction with PES-2.[18]

Table 2 shows a comparison of the pure rotational energies ($J \leq 5$) of CH_3 before and after refinement of r_e illustrating the importance of this step.

Table 2. Theoretical Rotational Term Values ($J \leq 5$, in cm^{-1}) of CH_3, Computed with TROVE Using Different Equilibrium Structure Parameters

states			term values		
N	K	τ_{rot}	obs.	obs. calc.[a]	obs. calc.[b]
1	1	0	14.3189	0.032377	0.004027
2	0	1	57.4396	0.112005	−0.002023
2	2	0	38.1186	0.092340	0.017004
2	1	0	52.6112	0.106875	0.002511
3	3	0	71.3965	0.179934	0.038989
3	2	0	95.5353	0.203902	0.014649
3	1	0	110.0032	0.219365	0.001200
4	0	0	191.2473	0.375024	−0.004034
4	4	0	114.1491	0.295456	0.070301
4	2	0	172.0038	0.353500	0.012772
4	3	0	147.9203	0.327970	0.035289

[a] Calculated using r_e = 1.07736927 Å and α_e = 120.0° (PES-1; see text). [b] Calculated using r_e = 1.0762977119 Å and α_e = 120.0° (PES-2; see text).

The vibrational transition moments are defined as

$$\mu_{V'V} = \sqrt{\sum_{\alpha=x,y,z} |\langle V'|\bar{\mu}_\alpha|V\rangle|^2} \tag{22}$$

where $|V'\rangle$ and $|V\rangle$ denote $J = 0$ vibrational wavefunctions and $\bar{\mu}_\alpha$ is the electronically averaged dipole moment in the molecular frame (see the section entitled "Dipole Moment Surface" above). For calculation of vibrational transition moments, we used our ab initio PES-1 and truncated the vibrational basis set at polyad number $P_{max} = 32$. A number of computed transition moments for the strongest lower lying bands are listed in Table 3 where they are compared with the available experimental data. The complete list of theoretical transition moments is given as Supporting Information and can be also found at www.exomol.com.

Table 3. Band Centers ν_{fi} and Vibrational Transition Moments μ_{fi} for CH_3[a]

states					
f	i	ν_{fi}/cm^{-1}	calc. μ_{fi}/D	obs. μ_{fi}/D	ref
$2\nu_2$	ν_2	678.81	0.25684	0.31(6)	40
ν_2	0	602.43	0.20403	0.215(25)	37, 39
ν_3^1	0	3158.83	0.03999	0.03(27)	63, 64
ν_4^1	0	1387.26	0.02931		
$2\nu_3 + \nu_4$	0	4529.74	0.02049		
$\nu_1 + \nu_4^1$	0	4383.56	0.00866		
$2\nu_2 + \nu_3^1$	0	4396.18	0.00486		
$2\nu_3^2$	0	6294.76	0.00462		
$\nu_1 + \nu_3^1$	0	6076.68	0.00321		
$2\nu_4^2$	0	2762.05	0.00313		
$\nu_3^1 + 2\nu_4$	0	5864.94	0.00242		
$3\nu_4^1$	0	4075.46	0.00186		
$2\nu_2 + \nu_3^1 + \nu_4^1$	0	5789.16	0.00130		
$4\nu_2$	0	5856.39	0.00116		

[a] The transitions originate in the vibrational ground state ($i = 0$) with the exception of the hot band $2\nu_2 \leftarrow \nu_2$.

Intensity Simulations. The simulation of absorption spectra at a given temperature T and within a particular wavenumber interval requires knowledge of the upper- and lower-state energies and the Einstein coefficients $A(f \leftarrow i)$ [or the line strengths $S(f \leftarrow i)$; the relationship between $A(f \leftarrow i)$ and $S(f \leftarrow i)$ is described in ref 55] for all transitions in the chosen wavenumber range. In practice, however, the transitions with intensities below a chosen limit are discarded. The most straightforward presentation of the spectral data is a "stick" diagram, with the stick heights representing the integrated absorption coefficients from eq 17. We report

DOI: 10.1021/acs.jpca.9b02919
J. Phys. Chem. A 2019, 123, 4755−4763

here such simulations for the CH_3 absorption bands in the wavenumber interval 600−1200 cm^{-1} for the out-of-plane bending mode ν_2. The line strengths in eq 17 are computed from eq 16 with the spin statistical weights g_{ns} from ref 18. The simulations are based on PES-2 and the computed DMS described above. The partition-function value used was Q = 732.734, obtained at 300 K as a summation over all variational term values ($J \leq 40$) below 36871.73 cm^{-1}. We have computed 2 058 655 166 transitions using the GPU GAIN-MPI program[59] within the various limits defined above.

Figure 2 gives an overview (log scale) of the absorption spectrum of CH_3 at different temperatures produced using the line list (log scale) by means of the ExoCross program.[65] Figure 3 shows four regions with the strongest, dipole-allowed bands ν_2, ν_4, ν_3, and $\nu_3 + \nu_4$.

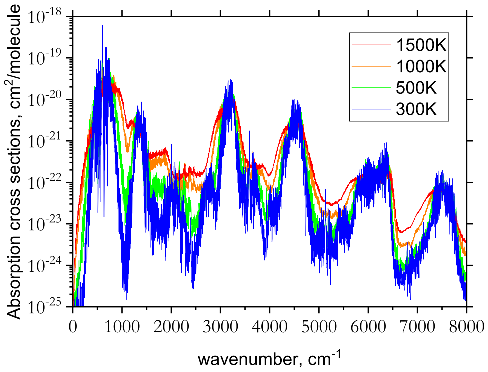

Figure 2. Overview of the absorption spectrum (cross sections) of CH_3 at different temperatures, T = 300, 500, 1000, and 1500 K, generated using our line list and the Gaussian line profile with the full width at half maximum (fwhm) of 2 cm^{-1}.

Figure 4 shows the emission spectrum of CH_3 in the wavenumber interval 600−1200 cm^{-1}, simulated with ExoCross at two different levels of theory, ro-vibrational and purely vibrational. The simulated spectra are compared to an experimental spectrum recorded by Hermann and Leone[66,67] (see Figure 4 of ref 66).

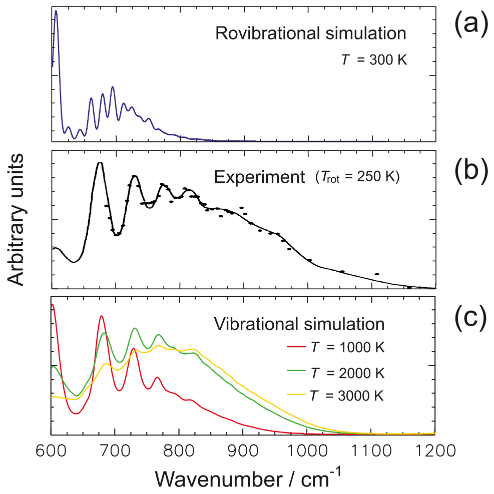

Figure 4. Emission spectra of CH_3. (a) Ro-vibrational simulation assuming the CH_3 radicals to be in thermal equilibrium at T = 300 K. (b) CH_3 (ν_2) out-of-plane bending mode emission spectrum (dots) obtained[66] after dissociation of $CH_3I \rightarrow CH_3(\nu_2) + I^*$. The continuous curve is the best fit[66] involving the hot bands $(v_2 + 1)\nu_2 \leftarrow v_2\nu_2$ with $v_2 \leq 9$. The spectrum is convolved with a spectrometer slit function with a fwhm of 33 cm^{-1} and a 19 cm^{-1} bandwidth ascribed to the breadth of the $\Delta K = 0$ manifold of transitions with varying J values. (c) Vibrational simulations at temperatures T = 1000, 2000, and 3000 K, respectively, taking into account the vibrational transitions $(v_2 + 1)\nu_2 \leftarrow v_2\nu_2$ with $v_2 \leq 9$ (see text). Panel (b) reproduced from Hermann, H. W.; Leone, S. R. *The Journal of Chemical Physics* 1982, 76, 4759−4765, with the permission of AIP Publishing.

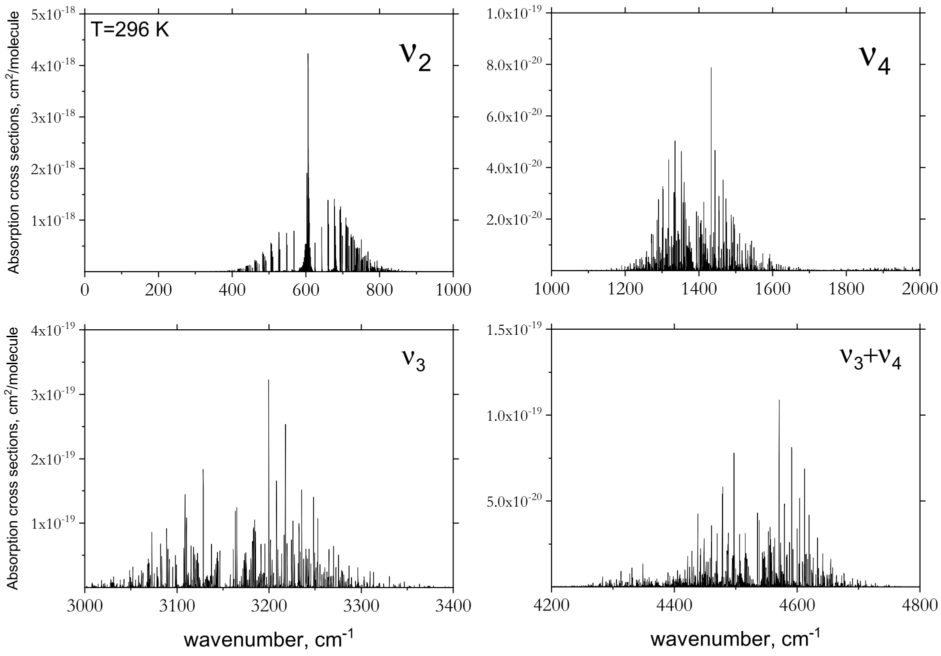

Figure 3. Selection of the strongest absorption bands of CH_3 at T = 296 K generated using the line list. A Gaussian line profile with the half width at half maximum of 0.08 cm^{-1} was used in the production of the cross sections shown.

DOI: 10.1021/acs.jpca.9b02919
J. Phys. Chem. A 2019, 123, 4755−4763

Figure 4(a) shows a simulation of the CH_3 emission spectrum, computed with ExoCross at a temperature of T = 300 K, taking into account all vibrational transitions in the 600−1200 cm^{-1} interval that are calculated with the P_{max} = 32 basis set. The simulation involves the convolution of the calculated intensities with a Gaussian line shape function with a fwhm of 34 cm^{-1}.

The simulation is compared with the experimental spectrum obtained by Hermann and Leone,[66,67] shown in Figure 4(b). In the experiment, the CH_3 radicals were produced in a photofragmentation process of methyl iodide CH_3I. Hermann and Leone[66,67] suggested that after the breaking of the C−I bond, the CH_3 radicals are predominantly produced in excited states of the out-of-plane bending mode ν_2. The CH_3 fragment of a dissociated CH_3I molecule will typically have a pyramidal structure close to that of the methyl group in CH_3I. For a CH_3 radical, however, which is planar at equilibrium, such structures are associated with high excitations of the ν_2 vibrational mode. Excitations with $v_2 \leq 10$ have been observed in the emission experiment of refs.[66,67]

In order to simulate vibrationally very hot transitions (hotter than 1500 K) corresponding to the experimental spectrum of ref 66, which involves out-of-plane bending states $v_2\nu_2$ with $v_2 \leq 10$, we have carried out simulations employing a so-called one-band model (with the one band being the ν_2 fundamental band here). In the one-band model, we use the ν_2-band data from the "parent", 300 K ro-vibrational line list also for the hot bands accompanying the ν_2 band. The procedure employed is detailed in ref 33 and we outline it briefly here: We initially produce the 300 K, ν_2-band cross sections by means of the ExoCross program[65] and convolve them with a Gaussian profile of fwhm = 34 cm^{-1} between 0 and 1200 cm^{-1}, generating 1201 data points. Then the wavenumbers of the computed cross sections are shifted by −606.4531 cm^{-1}, positioning the band center at zero, and the cross sections are normalized. A local version of ExoCross now obtains, from the vibrational transition moments computed with TROVE, the vibrational band intensities for the hot bands $(v_2 + 1)\nu_2 \leftarrow v_2\nu_2$, $v_2 \leq 9$. Finally, the simulated spectrum is generated by placing, for each hot band, the ν_2-band profile at the band center ν_{fi} of the hot band in question, scaled by its vibrational band intensity. Such simulations have been carried out for temperatures of 1000, 2000, and 3000 K, respectively, and the results are shown in Figure 4(c), where they can be compared to the experimental results[66,67] in Figure 4(b).

Figure 4 shows that the "standard" T = 300 K ro-vibrational simulation of the CH_3 emission spectrum [Figure 4(a)] has little resemblance to the experimental spectrum from ref 66 [Figure 4(b)]. Obviously, in the experiment, the CH_3 molecules populate states of much higher energies than those accessed in thermal equilibrium at T = 300 K. However, among the "vibrational simulations" in Figure 4(c), the curve obtained for T = 2000 K has a very substantial similarity to the experimental curve. This confirms the suggestion by Hermann and Leone[66,67] that dissociation of CH_3I produces CH_3 radicals in highly excited states of the out-of-plane bending mode ν_2. The successful simulation of the emission spectrum of refs[66,67] lends credibility to the ab initio DMS of the present work; the intensities based on this DMS are in very good qualitative agreement with experiment.

Our complete T = 1500 K CH_3 line list is accessed via the repository www.zenodo.org, see Accession Codes. It provides transition energies, line strengths, Einstein coefficients $A(\mathrm{f} \leftarrow \mathrm{i})$, and the temperature-dependent partition function $Q(T)$. We expect the line list to be applicable for temperatures below 1500 K. However, the simulated spectra will become increasingly inaccurate with increasing temperature. The line list is given in the ExoMol format,[20] which can be used together with the ExoCross program[65] to generate spectra of CH_3.

■ CONCLUSIONS

We report here simulations of spectra for the methyl radical, extending over a significant portion of the infrared spectral region. The positions and intensities calculated for the transitions are in excellent agreement with experiment, as demonstrated by detailed comparisons with observed room-temperature spectra.

The CH_3 line list of the present work will facilitate detections of the methyl radical in space. In the present work, we have generated, refined, and validated the potential energy and DMSs required for the spectral simulations, and we have established the level of accuracy attainable in variational nuclear-motion calculations with our computational resources. We have produced a methyl radical line list consisting of 2 billion transitions between 9 127 123 energy levels for rovibrational states up to J_{max} = 40 and energies up to 19 000 cm^{-1}.

■ ASSOCIATED CONTENT

Supporting Information

The Supporting Information is available free of charge on the ACS Publications website at DOI: 10.1021/acs.jpca.9b02919.

Fortran routines for calculating the dipole moment and potential energy values for given geometry (TXT)

Potential energy parameters $f^{(s)}_{jk\ldots}$ (TXT)

Dipole moment parameters $\mu^{(\Gamma)}_{k,l,m,\ldots}$ (TXT)

Ab initio potential parameters for the electronic ground state of CH_3 (TXT)

Accession Codes

The complete IR line list (states file, transition files with Einstein A coefficients, and partition function) for CH_3 can be accessed via the Zenodo repository at https://doi.org/10.5281/zenodo.2607732 as well as at www.exomol.com.

■ AUTHOR INFORMATION

Corresponding Author

*E-mail: jensen@uni-wuppertal.de.

ORCID

Sergei N. Yurchenko: 0000-0001-9286-9501

Per Jensen: 0000-0001-5133-7621

Notes

The authors declare no competing financial interest.

■ ACKNOWLEDGMENTS

A.Y. acknowledges support from DESY (HGF IVF). S.Y. is grateful for support from the UK Science and Technology Research Council (STFC) ST/R000476/1. This work made extensive use of UCL's Legion high performance (HPC) computing facilities as well as of HPC provided by DiRAC supported by STFC and BIS. It was further supported in part by grant JE 144/25-1 from the Deutsche Forschungsgemeinschaft.

REFERENCES

(1) Miller, J.; Kee, R. J.; Westbrook, C. K. Chemical Kinetics and Combustion Modeling. *Annu. Rev. Phys. Chem.* **1990**, *41*, 345−387.

(2) Ravishankara, A. R. Kinetics of Radical Reactions in the Atmospheric Oxidation of CH4. *Annu. Rev. Phys. Chem.* **1988**, *39*, 367−394.

(3) Jasinski, J.; Meyerson, B. S.; Scott, B. A. Mechanistic Studies of Chemical Vapor Deposition. *Annu. Rev. Phys. Chem.* **1987**, *38*, 109−140.

(4) Celii, F.; Butler, J. E. Diamond Chemical Vapor Deposition. *Annu. Rev. Phys. Chem.* **1991**, *42*, 643−684.

(5) Zhitnikov, R. A.; Dmitriev, Y. A. Detection of Free Radicals in Low-Temperature Gas-Grain Reactions of Astrophysical Interest. *Astron. Astrophys.* **2002**, *386*, 1129−1138.

(6) Feuchtgruber, H.; Moses, J. I.; Encrenaz, T. Detection of Methyl Radicals CH_3 on Saturn. *Astron. Astrophys.* **1998**, *44*, L41−L44.

(7) Bezard, B.; Romani, P. N.; Feuchtgruber, H.; Encrenaz, T. Detection of the Methyl Radical on Neptune. *Astrophys. J.* **1999**, *515*, 868−872.

(8) Feuchtgruber, H.; Helmich, F. P.; van Dishoeck, E. F.; Wright, C. M. Detection of Interstellar CH_3. *Astrophys. J.* **2000**, *535*, L111−L114.

(9) Settersten, T. B.; Farrow, R. L.; Gray, J. A. Coherent Infrared-Ultraviolet Double-Resonance Spectroscopy of CH_3. *Chem. Phys. Lett.* **2003**, *370*, 204−210.

(10) Tan, L. Y.; Pimentel, G. C. Infrared Spectrum of Gaseous Methyl Radical by Rapid Scan Spectroscopy. *J. Chem. Phys.* **1972**, *57*, 4028−4037.

(11) Holt, P. L.; McCurdy, K. E.; Weisman, R. B.; Adams, J. S.; Engel, P. S. Transient CARS Spectroscopy of the ν_1 Band of Methyl Radical. *J. Chem. Phys.* **1984**, *81*, 3349−3350.

(12) Kelly, P. B.; Westre, S. G. Resonance Raman Spectroscopy of the Methyl Radical. *Chem. Phys. Lett.* **1988**, *151*, 253−257.

(13) Triggs, N. E.; Zahedi, M.; Nibler, J. W.; DeBarber, P.; Valentini, J. J. High Resolution Study of the ν_1 Vibration of CH_3 by Coherent Raman Photofragment Spectroscopy. *J. Chem. Phys.* **1992**, *96*, 1822−1831.

(14) Zahedi, M.; Harrison, J. A.; Nibler, J. W. 266 nm CH_3I Photodissociation: CH_3 Spectra and Population Distributions by Coherent Raman Spectroscopy. *J. Chem. Phys.* **1994**, *100*, 4043−4055.

(15) Hädrich, S.; Hefter, S.; Pfelzer, B.; Doerk, T.; Jauernik, P.; Uhlenbusch, J. Determination of the Absolute Raman Cross Section of Methyl. *Chem. Phys. Lett.* **1996**, *256*, 83−86.

(16) Westre, S. G.; Kelly, P. B. Examination of CD_3 Vibrational Structure by Resonance Raman Spectroscopy. *J. Chem. Phys.* **1989**, *90*, 6977−6979.

(17) Miller, J. T.; Burton, K. A.; Weisman, R. B.; Wu, W.-X.; Engel, P. S. CARS Spectroscopy of Gas Phase CD_3. *Chem. Phys. Lett.* **1989**, *158*, 179−183.

(18) Adam, A. Y.; Yachmenev, A.; Yurchenko, S. N.; Jensen, P. Ro-Vibrational Averaging of the Isotropic Hyperfine Coupling Constant for the Methyl Radical. *J. Chem. Phys.* **2015**, *143*, 244306.

(19) Tennyson, J.; Yurchenko, S. N. ExoMol: Molecular Line Lists for Exoplanet and Other Atmospheres. *Mon. Not. R. Astron. Soc.* **2012**, *425*, 21−33.

(20) Tennyson, J.; Yurchenko, S. N.; Al-Refaie, A. F.; Barton, E. J.; Chubb, K. L.; Coles, P. A.; Diamantopoulou, S.; Gorman, M. N.; Hill, C.; Lam, A. Z.; et al. The ExoMol Database: Molecular Line Lists for Exoplanet and Other Hot Atmospheres. *J. Mol. Spectrosc.* **2016**, *327*, 73−94.

(21) Yurchenko, S. N.; Tennyson, J. ExoMol Line Lists IV: The Rotation-Vibration Spectrum of Methane Up to 1500 K. *Mon. Not. R. Astron. Soc.* **2014**, *440*, 1649−1661.

(22) Yurchenko, S. N.; Barber, R. J.; Yachmenev, A.; Thiel, W.; Jensen, P.; Tennyson, J. A Variationally Computed T=300 K Line List for NH3. *J. Phys. Chem. A* **2009**, *113*, 11845−11855.

(23) Sousa-Silva, C.; Hesketh, N.; Yurchenko, S. N.; Hill, C.; Tennyson, J. High Temperature Partition Functions and Thermodynamic Data for Ammonia and Phosphine. *J. Quant. Spectrosc. Radiat. Transfer* **2014**, *142*, 66−74.

(24) Sousa-Silva, C.; Al-Refaie, A. F.; Tennyson, J.; Yurchenko, S. N. ExoMol Line Lists - VII. The Rotation-Vibration Spectrum of Phosphine Up to 1500 K. *Mon. Not. R. Astron. Soc.* **2015**, *446*, 2337−2347.

(25) Underwood, D. S.; Yurchenko, S. N.; Tennyson, J.; Jensen, P. Rotational Spectrum of SO_3 and Theoretical Evidence for the Formation of Rotational Energy Level Clusters in its Vibrational Ground State. *J. Chem. Phys.* **2014**, *140*, 244316.

(26) Underwood, D. S.; Yurchenko, S. N.; Tennyson, J.; Al-Refaie, A. F.; Clausen, S.; Fateev, A. ExoMol Line Lists XVII: A Line List for Hot SO_3. *Mon. Not. R. Astron. Soc.* **2016**, *462*, 4300−4313.

(27) Al-Refaie, A. F.; Yachmenev, A.; Tennyson, J.; Yurchenko, S. N. ExoMol Line Lists - VIII: A Variationally Computed Line List for Hot Formaldehyde. *Mon. Not. R. Astron. Soc.* **2015**, *448*, 1704−1714.

(28) Owens, A.; Yurchenko, S. N.; Yachmenev, A.; Tennyson, J.; Thiel, W. Accurate *ab initio* Vibrational Energies of Methyl Chloride. *J. Chem. Phys.* **2015**, *142*, 244306.

(29) Owens, A.; Yachmenev, A.; Thiel, W.; Tennyson, J.; Yurchenko, S. N. ExoMol Molecular Line Lists XXII. The Rotation-Vibration Spectrum of Silane Up to 1200 K. *Mon. Not. R. Astron. Soc.* **2017**, *471*, 5025−5032.

(30) Al-Refaie, A. F.; Ovsyannikov, R. I.; Polyansky, O. L.; Yurchenko, S. N.; Tennyson, J. A Variationally Calculated Room Temperature Line-List for H_2O_2. *J. Mol. Spectrosc.* **2015**, *318*, 84−90.

(31) Al-Refaie, A. F.; Polyansky, O. L.; Ovsyannikov, R. I.; Tennyson, J.; Yurchenko, S. N. ExoMol Line Lists XV: A Hot Line List for Hydrogen Peroxide. *Mon. Not. R. Astron. Soc.* **2016**, *461*, 1012−1022.

(32) Chubb, K. L.; Yachmenev, A.; Tennyson, J.; Yurchenko, S. N. Treating Linear Molecule HCCH in Calculations of Rotation-Vibration Spectra. *J. Chem. Phys.* **2018**, *149*, 014101.

(33) Mant, B. P.; Yachmenev, A.; Tennyson, J.; Yurchenko, S. N. ExoMol Molecular Line Lists - XXVII: Spectra of C_2H_4. *Mon. Not. R. Astron. Soc.* **2018**, *478*, 3220−3232.

(34) Gordon, I. E.; Rothman, L. S.; Hill, C.; Kochanov, R. V.; Tan, Y.; Bernath, P. F.; Birk, M.; Boudon, V.; Campargue, A.; Chance, K. V.; et al. The HITRAN2016 Molecular Spectroscopic Database. *J. Quant. Spectrosc. Radiat. Transfer* **2017**, *203*, 3−69.

(35) Bunker, P. R.; Jensen, P. *Molecular Symmetry and Spectroscopy*, 2nd ed.; NRC Research Press: Ottawa, 1998; p 748.

(36) Hudgens, J. W.; DiGiuseppe, T. G.; Lin, M. C. Two Photon Resonance Enhanced Multiphoton Ionization Spectroscopy and State Assignments of the Methyl Radical. *J. Chem. Phys.* **1983**, *79*, 571−582.

(37) Yamada, C.; Hirota, E. The Transition Dipole Moment of the ν_2 Band of the Methyl Radical. *J. Chem. Phys.* **1983**, *78*, 669−671.

(38) Wormhoudt, J.; McCurdy, K. E. A measurement of the strength of the ν_2 band of CH_3. *Chem. Phys. Lett.* **1989**, *156*, 47−50.

(39) Stancu, G. D.; Röpcke, J.; Davies, P. B. Line Strengths and Transition Dipole Moment of the ν_2 Fundamental Band of the Methyl Radical. *J. Chem. Phys.* **2005**, *122*, 014306.

(40) Stancu, G. D.; Röpcke, J.; Davies, P. B. Measurement of the Transition Dipole Moment of the First Hot Band of the ν_2 Mode of the Methyl Radical by Diode Laser Spectroscopy. *J. Phys. Chem. A* **2008**, *112*, 6285−6288.

(41) Yurchenko, S. N.; Carvajal, M.; Jensen, P.; Lin, H.; Zheng, J.; Thiel, W. RotationVibration Motion of Pyramidal XY3 Molecules Described in the Eckart Frame: Theory and Application to NH_3. *Mol. Phys.* **2005**, *103*, 359−378.

(42) Yurchenko, S. N.; Thiel, W.; Jensen, P. Theoretical ROVibrational Energies (TROVE): A Robust Numerical Approach to the Calculation of Rovibrational Energies for Polyatomic Molecules. *J. Mol. Spectrosc.* **2007**, *245*, 126−140.

(43) Yachmenev, A.; Yurchenko, S. N. Automatic Differentiation Method for Numerical Construction of the Rotational-Vibrational Hamiltonian as a Power Series in the Curvilinear Internal Coordinates Using the Eckart Frame. *J. Chem. Phys.* **2015**, *143*, 014105.

(44) Yurchenko, S. N.; Yachmenev, A.; Ovsyannikov, R. I. Symmetry-Adapted Ro-vibrational Basis Functions for Variational Nuclear Motion Calculations: TROVE Approach. *J. Chem. Theory Comput.* **2017**, *13*, 4368−4381.

(45) Adler, T. B.; Knizia, G.; Werner, H.-J. A Simple and Efficient CCSD(T)-F12 Approximation. *J. Chem. Phys.* **2007**, *127*, 221106.

(46) Adler, T. B.; Werner, H.-J. Local Explicitly Correlated Coupled-Cluster Methods: Efficient Removal of the Basis Set Incompleteness and Domain Errors. *J. Chem. Phys.* **2009**, *130*, 241101.

(47) Peterson, K. A.; Adler, T. B.; Werner, H.-J. Systematically Convergent Basis Sets for Explicitly Correlated Wavefunctions: The Atoms H, He, B-Ne, and Al-Ar. *J. Chem. Phys.* **2008**, *128*, 084102.

(48) Yachmenev, A.; Yurchenko, S. N.; Ribeyre, T.; Thiel, W. High-Level ab initio Potential Energy Surfaces and Vibrational Energies of H_2C_S. *J. Chem. Phys.* **2011**, *135*, 074302.

(49) Lin, H.; Thiel, W.; Yurchenko, S. N.; Carvajal, M.; Jensen, P. Vibrational Energies for NH_3 Based on High Level *ab initio* Potential Energy Surfaces. *J. Chem. Phys.* **2002**, *117*, 11265−11276.

(50) Werner, H.-J.; Knowles, P. J.; Knizia, G.; Manby, F. R.; Schütz, M. Molpro: A General-Purpose Quantum Chemistry Program Package. *Wiley Interdiscip. Rev.: Comput. Mol. Sci.* **2012**, *2*, 242−253.

(51) Watts, J. D.; Gauss, J.; Bartlett, R. J. Coupled-Cluster Methods with Noniterative Triple Excitations for Restricted Open-Shell Hartree−Fock and Other General Single Determinant Reference Functions. Energies and Analytical radients. *J. Chem. Phys.* **1993**, *98*, 8718−8733.

(52) Dunning, T. H. Gaussian Basis Sets for Use in Correlated Molecular Calculations. I. The Atoms Boron through Neon and Hydrogen. *J. Chem. Phys.* **1989**, *90*, 1007−1023.

(53) Kendall, R. A.; Dunning, T. H., Jr.; Harrison, R. J. Electron Affinities of the First-Row Atoms Revisited. Systematic Basis Sets and Wave Functions. *J. Chem. Phys.* **1992**, *96*, 6796−6806.

(54) Yurchenko, S. N.; Carvajal, M.; Lin, H.; Zheng, J.; Thiel, W.; Jensen, P. Dipole Moment and Rovibrational Intensities in the Electronic Ground state of NH_3: Bridging the Gap Between *ab initio* Theory and Spectroscopic Experiment. *J. Chem. Phys.* **2005**, *122*, 104317.

(55) Yurchenko, S. N.; Thiel, W.; Carvajal, M.; Lin, H.; Jensen, P. Rotation-Vibration Motion of Pyramidal XY3 Molecules Described in the Eckart Frame: The Calculation of Intensities with Application to NH_3. *Adv. Quantum Chem.* **2005**, *48*, 209−238.

(56) Bunker, P. R.; Jensen, P. *The Fundamentals of Molecular Symmetry*, 1st ed.; CRC Press: Boca Raton, 2004; p 358.

(57) Špirko, V.; Bunker, P. R. The Potential Function and Rotation-Vibration Energy Levels of the Methyl Radical CH_3. *J. Mol. Spectrosc.* **1982**, *95*, 381−390.

(58) Davis, S.; Anderson, D. T.; Duxbury, G.; Nesbitt, D. J. J. Jet-Cooled Molecular Radicals in Slit Supersonic Discharges: Sub-Doppler Infrared Studies of Methyl Radical. *J. Chem. Phys.* **1997**, *107*, 5661−5675.

(59) Al-Refaie, A. F.; Yurchenko, S. N.; Tennyson, J. GPU Accelerated Intensities MPI GAIN-MPI: A New Method of Computing Einstein-A Coefficients. *Comput. Phys. Commun.* **2017**, *214*, 216−224.

(60) Ovsyannikov, R. I.; Thiel, W.; Yurchenko, S. N.; Carvajal, M.; Jensen, P. Vibrational Energies of PH_3 Calculated Variationally at the Complete Basis Set Limit. *J. Chem. Phys.* **2008**, *129*, 044309.

(61) Yamada, C.; Hirota, E.; Kawaguchi, K. Diode Laser Study of the ν_2 Band of the Methyl Radical. *J. Chem. Phys.* **1981**, *75*, 5256−5264.

(62) Jacox, M. E. *Vibrational and Electronic Energy Levels of Polyatomic Transient Molecules. Supplement B*; American Chemical Society: New York, 2005; Vol. *1*.

(63) Bethardy, G. A.; Macdonald, R. G. Direct Measurement of the Transition Dipole Moment of the ν_3 Asymmetric C-H Stretching Vibration of the CH_3 Radical. *J. Chem. Phys.* **1995**, *103*, 2863−2872.

(64) Tanarro, I.; Sanz, M. M.; Domingo, C.; Bermejo, D.; Santos, J.; Domenech, J. L. Transition Dipole Moment of the ν_3 Band of CH_3. *J. Phys. Chem.* **1994**, *98*, 5862−5866.

(65) Yurchenko, S. N.; Al-Refaie, A. F.; Tennyson, J. ExoCross: A General Program for Generating Spectra from Molecular Line Lists. *Astron. Astrophys.* **2018**, *614*, A131.

(66) Hermann, H. W.; Leone, S. R. Photofragment Infrared Emission Spectroscopy: Vibrational Progression and Potential Parameters of the $CH_3(\nu_2)$ Umbrella" Mode. *J. Chem. Phys.* **1982**, *76*, 4759−4765.

(67) Hermann, H. W.; Leone, S. R. Photofragmentation Dynamics of CH_3I at 248 and 266 nm: Vibrational Distributions in the $CH_3(\nu_2)$ Umbrella" Mode. *J. Chem. Phys.* **1982**, *76*, 4766−4774.